LOW-TEMPERATURE
PLASMA

Formation of Extended Tubular Plasma in Argon at Low Pressure and in a Weak Longitudinal Magnetic Field

Yu. S. Akishev[a,b,*], **V. P. Bakhtin**[a], **A. B. Buleyko**[a], **O. T. Loza**[a], **A. V. Petryakov**[a],
A. A. Ravaev[a], **and E. A. Fefelova**[a]

[a]*Troitsk Institute for Innovative and Thermonuclear Research, Moscow, 108840 Russia*
[b]*National Research Nuclear University "Moscow Engineering Physics Institute," Moscow, 115409 Russia*
e-mail: akishev@triniti.ru

Abstract—The results of experimental studies on the formation and subsequent evolution of extended ($l = 300$ mm) and thin-walled ($\Delta r \approx 10$ mm) tubular ($2r \approx 110$ mm) plasma in a weak longitudinal magnetic field ($B = 175$ G) without the use of a thermionic cathode are presented. The cylindrical chamber in which the tubular plasma was formed was pumped with high purity argon (99.998%) at an average velocity of about 1 m/s at a pressure of $P = 10^{-3}-10^{-2}$ Torr. Two methods of creating seed electrons initiating the development of ionization avalanches were used. The difference inherent to these methods has been established in the dynamics of breakdown, completing in the formation of a tubular discharge. In the first of them, a pulsed discharge preceding the high voltage supply of the main discharge created gas preionization in a small area around the sectioned cathodes. In the second method, seed electrons were created in the entire working area of the discharge chamber by an RF discharge with a frequency of 85 kHz and duration of about 1 s. High-speed shooting with a 4-frame ICCD camera allowed us to establish the dynamics of tubular discharge formation at all its stages. Measurements of the longitudinal and radial discharge current were carried out. The results we obtained showed the possibility of spatial isolation of an extended tubular plasma from the close located metal wall of the discharge chamber by using a weak longitudinal magnetic field.

1. INTRODUCTION

There is interest in microwave radiation sources based on a plasma maser. A plasma maser is a device in which microwave radiation occurs as a result of the Cherenkov interaction of a high-current relativistic electron beam with an extended plasma created in a rarefied inert gas at a pressure of $P = 10^{-2}-10^{-3}$ Torr [1]. The most common plasma masers are of the coaxial type, in which both the electron beam and the plasma have a tubular shape [2–5]. A thermionic cathode is used to form tubular plasma [2–4]. Thoriated tungsten is usually used as the material of the thermionic cathode. When a negative voltage pulse is applied to the incandescent cathode, the thermoemissive electrons are accelerated by an electric field and ionize the working gas in the discharge chamber. This process takes place in a strong longitudinal magnetic field, which keeps the plasma from contacting the nearby metal wall. The thickness and radius of the formed plasma cylinder are determined by the size of the thermocathode and the magnitude of the magnetic field. In this case, the thermocathode works not only as an

emitter of seed electrons, which initiate an ionization wave propagating from the cathode to the anode, but also as a normal cathode collecting a large current of ions from the plasma created by the discharge. Due to this, a cathode layer is formed at the surface of the thermocathode, in which positive ions coming from the plasma begin to play a dominant role. First, they neutralize the negative space charge of electrons near the emissive cathode and thereby eliminate its current regime with a volt−ampere characteristic corresponding to the Child−Langmuir law (the 3/2 law). Second, the ions accelerated in the cathode layer are able to strongly modify the cathode surface. This modification can change the microstructure of thin layer of the cathode surface. Due to this, the cathode work function can increase that leads to a decrease in the cathode emissive capability. Such an effect is observed in experiments.

In addition, at discharge currents on the cathode of more than a few amperes, pre-arc [6] or arc [7] cathode spots with very high current density (10^6 A/cm² and higher) can form. The high level of local energy
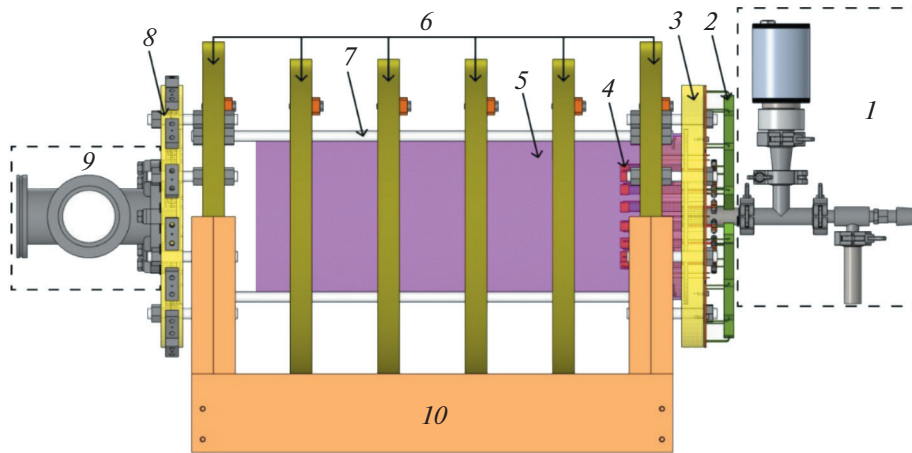
Fig. 1. A sketch of the GDC with Helmholtz coils (side view). (*1*) The gas inlet system; (*2*) the cathode ballast resistor *R*; (*3*) the cathode end flange on which a sectioned cathode of 16 separate cathodes is mounted; (*4*) the cathode and auxiliary anode; (*5*) the thin metal mesh inside a quartz tube, pressed closely against its inner wall; (*6*) the Helmholtz coils creating a longitudinal magnetic field with an induction of 175 G; (*7*) the quartz tube with a diameter of 200 mm, inside which a system of electrodes is mounted to create a tubular plasma; (*8*) the anode end flange; (*9*) the ISO63 cross for connection with vacuum system; (*10*) the mounting bracket for GDC and Helmholtz coils.

release in the cathode spot creates a high local temperature on the cathode surface. Extremely high temperatures lead to thermal restructuring of the thermocathode material in its entire thickness. As a result, embrittlement of the thermocathode occurs. Embrittlement is a destructive effect because it greatly reduces the mechanical strength of the thermocathode and leads to its complete destruction even from weak external shocks. Especially, embrittlement is a danger for thin wire or foil thermocathodes, which are usually used in plasma masers. For these reasons, the development of methods for creating tubular plasma without the use of a thermocathode is a relevant but a difficult task. Its complexity is additionally increased due to the requirement to create extended plasma near a metal wall using a weak magnetic field, which has to be several tens of times lower than that commonly used in plasma masers.

Various plasma devices have been developed; the robust breakdown stability and plasma formation in them are based on the use of gas preionization by an auxiliary surface or volume discharge. As a rule, auxiliary discharges create seed electrons near the cathode [8]. This article presents the results of experimental studies on the dynamics of formation and subsequent evolution of extended (l = 30 cm) and thin-walled ($\Delta r \approx$ 1 cm) tubular plasma near a metal wall in a weak longitudinal magnetic field (B = 175 G) without using a thermionic cathode, but with use of local (near cathodes) and global (in the entire volume of the gas discharge chamber) preionization.

2. EXPERIMENTAL

The study of the peculiarities of the formation of tubular plasma without the use of a thermionic cathode was carried out on a setup; a sketch of it is shown in Fig. 1. This setup includes a gas discharge chamber (GDC), as well as the necessary equipment for the formation of auxiliary and main discharges and diagnostics of the created tubular plasma. High purity argon was used as the working gas. Before each experiment, the GDC was pumped to a pressure of P = 10^{-5} Torr. The gas discharge chamber is placed inside six Helmholtz coils, which create a weak longitudinal magnetic field. The current passed through the coils determines the magnitude of the magnetic induction. The experiments were carried out at a magnetic induction magnitude equal to 175 G. Magnetic induction measurements have shown that the magnetic field is fairly uniform both along and across the discharge. The induction was measured by a Honeywell SS494B Hall sensor with a sensitivity of 5 mV/G and with dimensions of $3 \times 4 \times 1$ mm^3.

The basis of the GDC is a long quartz tube (L = 600 mm) with a wall thickness of 4 mm and an internal diameter of 192 mm, inside which a system of electrodes is mounted to create a tubular plasma. The cathode of the plasma source is sectioned and consists of several cathode elements evenly spaced around a circle with a diameter of 110 mm. The number of cathode elements is determined by the required degree of plasma uniformity in the azimuthal direction. The design of the GDC enables one to change the number of cathode elements and increase their number up to 16. Each cathode element was connected to a high voltage source (capacitor with a capacity of C = 5 μF)

through an individual ballast resistor R; the value of the main discharge current depends on it. The duration of the current was determined by RC. The cathode connection scheme also provided ignition of an auxiliary discharge along the dielectric surface around each cathode element.

The anode (current collector) also consists of a set of anode elements evenly spaced around a circle with a diameter of 110 mm and located strictly opposite the cathode elements. The anode elements are shorted to each other and connected to the ground via a current shunt. The distance between the sectioned cathode and the current collector was chosen to be 30 cm, but the design of the system allowed this to be changed.

A thin and transparent metal mesh is placed immediately adjacent to the inner wall of the quartz tube, imitating the solid metal wall of the discharge chamber. The motivation for using the grid was that to date there is no information in the literature about the structure of the tubular plasma inside the maser during both plasma formation and its further maintenance by discharge current. The reason for this is that to generate intense microwave radiation, the metal body of a plasma maser should not have any holes through which it would be possible to observe the created plasma. The presence of holes can lead to a significant change in the conditions of generation and the mode structure of the output radiation.

In our case, the cells of the thin grid were 0.8×0.8 mm^2 in size, thus, the grid had a geometric transparency of at least 70%. Such transparency is quite sufficient to record the three-dimensional dynamics of the tubular plasma formation with a fast optical camera under different experimental parameters, for instance, immediately after a high-voltage pulse is applied to the cathode elements and the further evolution of the plasma structure. The inhomogeneity of the electric field, due to the cellular structure of the grid, exists only in the vicinity of the grid and extends from the grid no further than the size of its cell. Under experimental conditions, the characteristic distance from the grid to the tubular plasma was much larger than the cell size. In this case, it can be argued that the fine-mesh grid imitated the solid metal wall of the maser quite well. In addition, the grid could either be short-circuited to the anode, or separately connected to the ground via a current shunt. Such a scheme allowed us to independently measure the currents separately collected by the grid and the anode and draw a conclusion about the degree of magnetic isolation of the tubular plasma from the metal wall of the maser.

Experiments on the tubular plasma formation were performed using two preionization methods that create seed electrons immediately before applying a high-voltage pulse of the main discharge. The first method is local, because it created preionizing plasma localized only around each cathode on an area of no more than 1 cm^2. The duration of the auxiliary discharge that created the preionizing plasma did not exceed 0.1 μs. The second method is nonlocal (global), because it created preionizing plasma by an auxiliary RF discharge in the entire working area of the GDC. An RF discharge with a frequency of 85 kHz and a voltage amplitude of no more than 2 kV was used. The high-voltage pulse of the main discharge was applied approximately 1 s after switching on the RF generator.

3. RESULTS

3.1. Formation of Tubular Plasma Due to the Creation of Seed Electrons by an Auxiliary Pulsed Discharge along the Dielectric Surface around the Cathodes

Initially, a study on the discharge formation was conducted with a single element of a multi-section cathode. It was found that the appearance of a single plasma filament oriented along the magnetic field occurs quite quickly, that is, within 5−6 μs after the occurrence of an auxiliary discharge around the selected cathode element. However, the auxiliary discharge itself does not occur immediately, but with a delay after applying a high voltage to the cathode element. A well, there is a noticeable variation in the duration of the delay with fixed experimental parameters.

A set of typical oscillograms of the voltage at the cathode U_c, the current of the auxiliary surface discharge I_{aux} and the currents to the grid I_g and the anode (collector) I_a is shown in Fig. 2. The current I_g is radial current perpendicular to the magnetic field; the current I_a is a longitudinal current parallel to the magnetic field. The amplitude of the applied voltage and the argon pressure in the GDC were equal to $U = 5$ kV and $P = 3 \times 10^{-3}$ Torr. From the above data, it can be seen that under the same experimental conditions, there is a variation in the delay in the appearance of the auxiliary discharge. An analysis of the entire array of experimental data showed that both the delay and the scatter in duration of the delay increase on average with a decrease in gas pressure and the amplitude of the applied voltage. In some cases, the delays were very significant. Thus, at a pressure of $P = 3 \times 10^{-3}$ Torr and $U = 5$ kV, the delay in the appearance of an auxiliary discharge could sometimes reach several milliseconds, and at the same pressure and a lower voltage of $U = 3.5$ kV, a delay of several tens of milliseconds was recorded.

One can see in Fig. 2a that the current I_a collected by the anode begins to increase sharply immediately after the appearance of an auxiliary surface discharge around the cathode. The subsequent decrease in the collector current happens due to a decrease in voltage on the discharging capacitor of $C = 5$ μF. If necessary, by increasing the capacity of this capacitor, the current drop can be slowed.

When more cathodes are connected to a voltage source, the statistics characterizing the occurrence of
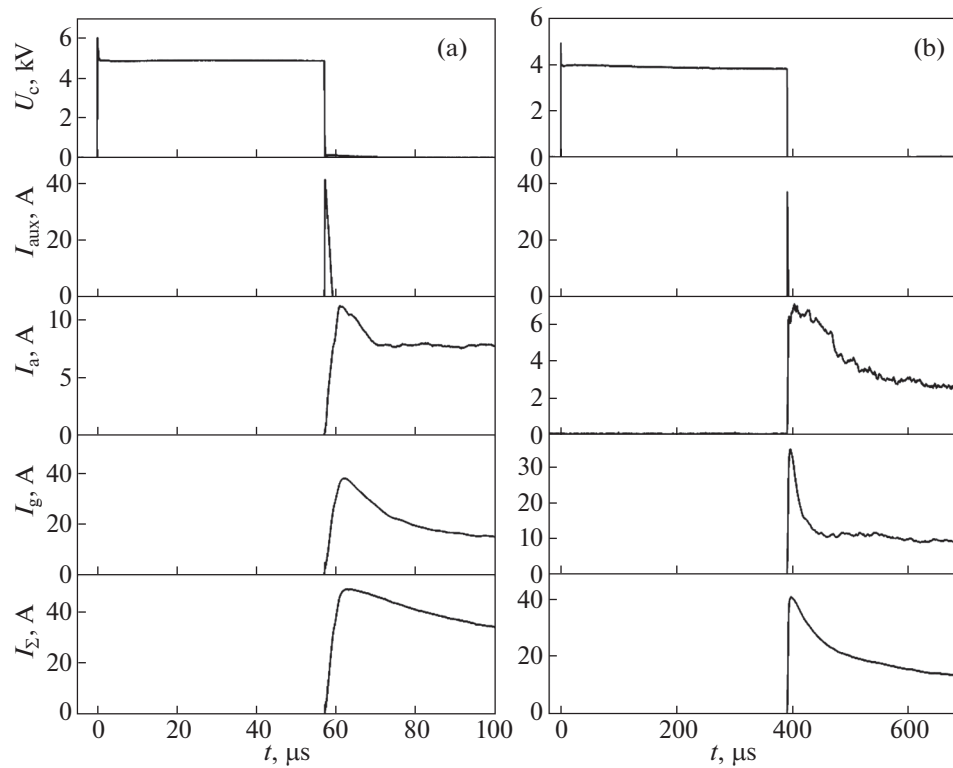
Fig. 2. The characteristic oscillograms of the voltage at the cathode U_c and the current of the auxiliary discharge I_{aux}, the current of the anode I_a, the current to the grid I_g, and the total current $I_\Sigma = I_a + I_g$ during the development of a single current filament. (a) Capacitor C is charged to 5 kV; (b) capacitor C is charged to 4 kV. Argon pressure $P = 3 \times 10^{-3}$ Torr.

auxiliary discharges at the cathodes changes significantly. The fact that auxiliary discharges do not occur simultaneously on all connected cathodes was quite expected. Another issue was unexpected: the average delay for the spontaneous occurrence of the very first auxiliary discharge on one of the collectively connected cathodes was noticeably reduced compared to the delay of the discharge on the same cathode if only it was connected. With the collective connection of the cathodes, the scatter in the duration of the delay in the occurrence of a discharge on each of the cathodes was noticeably reduced. With simultaneous connection of all cathodes, the average delay time at each cathode was in the range of 55 ± 35 μs, which sharply contrasts with delays of several milliseconds or even tens of milliseconds typical for single-connected cathodes.

The next issue was that after the spontaneous occurrence of the very first auxiliary surface discharge around one of the cathodes there was a rapid occurrence of surface discharges around neighboring cathodes. Thus, a spontaneous surface breakdown at one of the cathodes remotely initiated a surface breakdown around neighboring cathodes. In turn, other electrodes initiated a breakdown at their neighbors and further. Eventually, this process led to the rapid occurrence of auxiliary discharges at all cathodes.

The characteristic propagation time of the wave of such remotely induced (forced) surface breakdowns was only a few microseconds. It turned out the distance between cathodes connected to high voltage is of great importance for the occurrence of this effect. If the cathodes were connected through one or two, i.e., the connected cathodes were further apart, the time of induced breakdown occurrence increased. At large distances between the connected cathodes, the effect of initiating breakdown disappeared. This effect was also greatly weakened by a decrease in the current per cathode element.

An illustration of this is shown in Fig. 3, which shows oscillograms of currents and voltages from four cathodes for two combinations of their connection. In Fig. 3a four neighbor cathodes are connected (the distance between their centers is 21 mm). In Fig. 3b four cathodes are also connected, but through two that were not connected to high voltage (in this case, the distance between the centers of the connected cathodes was 63 mm).

As can be seen in Fig. 3a, the delay in the spontaneous occurrence of a surface discharge at the very first triggered cathode is 21 μs after a high-voltage pulse is applied to the cathodes. During the next 4 μs, an initiated (forced) surface breakdown occurs around the remaining cathodes. The same values for the sec-
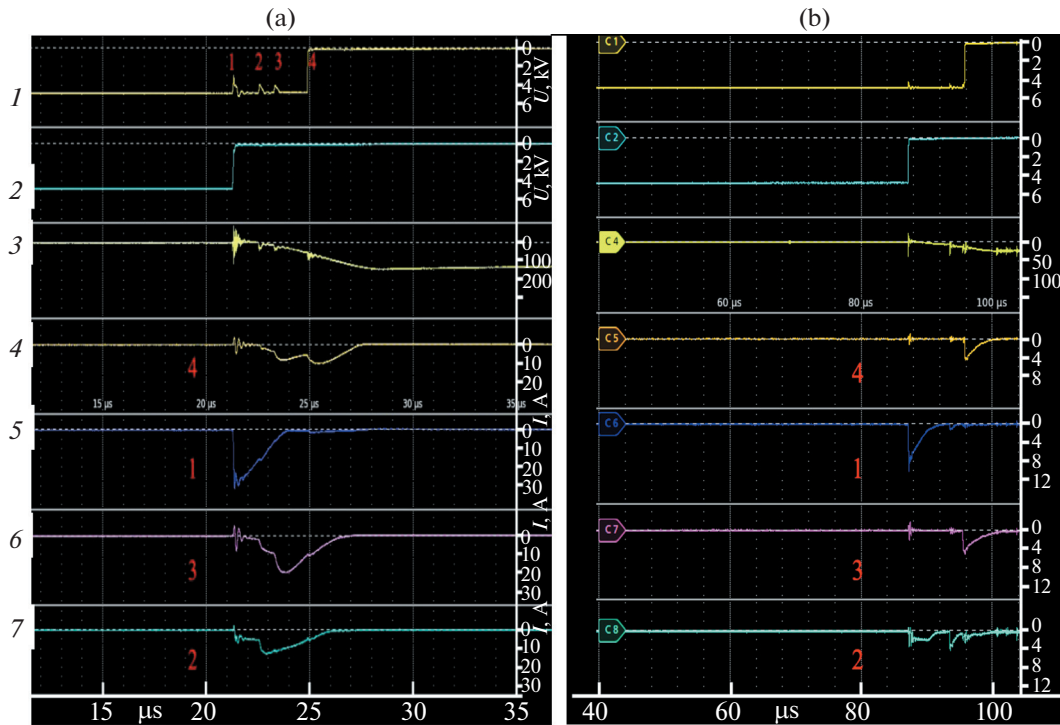
Fig. 3. Waveforms of the currents and voltages when four neighbor cathodes are connected. The first and second lines are voltage waveforms at the fourth and first cathodes (the numbering of the cathodes is according to the time of their breakdown formation), the third line is the anode current, the fourth—seventh lines are the currents of auxiliary discharges of the fourth, first, third and second cathodes.

ond option of connecting four cathodes (Fig. 3b) are 87 and 8 μs, respectively. High-speed imaging of the process confirmed these measurements: the time required to form a plasma cylinder did not exceed 90 μs when even the maximum number of cathode elements were connected. After extended tubular plasma formation the voltage drop along the entire plasma cylinder was small ($U \approx 100 \pm 20$ V). As a conclusion to this section, one can state that the first (local) method of creating preionization provided the formation of tubular plasma in argon at pressures in the range 3×10^{-2}–3×10^{-3} Torr and amplitudes of the applied voltage from 3 to 5 kV, but with a delay of 20 to 90 μs.

3.2. Formation of Tubular Plasma during the Creation of Seed Electrons by an Auxiliary High-frequency Discharge in the Entire Volume of the GDC

In the second (nonlocal) method of creating seed electrons, the RF voltage was applied either to a separately selected cathode or to all cathodes simultaneously. The amplitude of the RF voltage was chosen from the condition that, on the one hand, this voltage ensures the creation of a low-concentration seed plasma, and, on the other hand, the amplitude should

not be high so as not to create a premature breakdown between the cathode and the anode.

3.2.1. The dynamics of the azimuthal structure of a single plasma filament. Studies of the tubular plasma formation during HF preionization also began with the study of a single plasma filament formation. In addition to recording the cathode voltage and discharge currents, in each experiment high-speed photoregistration of the process was performed with recording of events in the entire volume of the GDC. This registration was carried out in a direction perpendicular to the axis of the gas discharge system. To study the dynamics of the azimuthal structure of the plasma filament, a cathode lying in a horizontal plane with the axis of the discharge chamber was selected.

Figure 4a shows five consecutive frames with images of the plasma filament development during the time $\Delta t \approx 0.1$ μs, when the total discharge current increases from zero to a maximum magnitude ($I_{max} \approx 25$ A). As can be seen, the plasma filament "tied" to the selected cathode element is displaced relative to the horizontal cathode—anode line. This is due to the combined action of the RF electric field and the longitudinal magnetic field, despite their relatively small values. We note that in the frame there is no pronounced front of the ionization wave directed towards the anode forming high conductivity in the plasma fil-
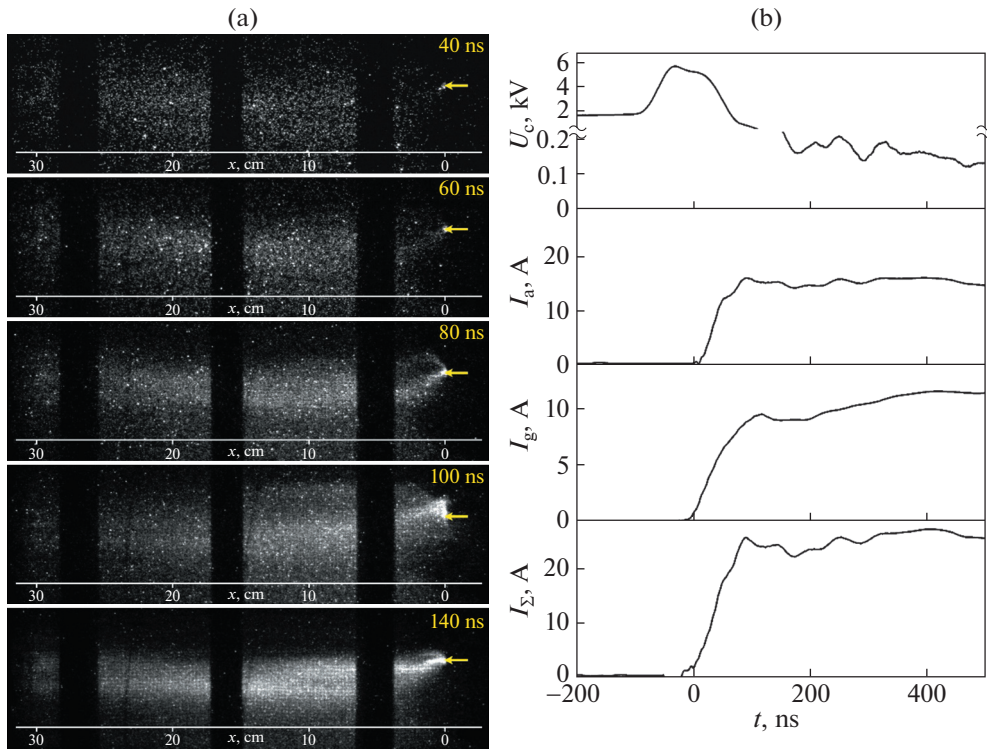
Fig. 4. (a) Five consecutive images of the plasma filament in the process of its development over a period of $\Delta t \approx 100$ ns. Dark vertical stripes on the frames are Helmholtz coils; yellow arrows show the position of the cathode; (b) oscillograms of voltage at the cathode U_c, currents to the grid I_g, anode I_a, and total current $I_\Sigma = I_g + I_a$.

ament. The front (if one can call it that) is strongly stretched and blurred in the longitudinal direction, so that in fact the filament conductivity is formed almost immediately along entire filament length, but with different intensities. At the same time, in the azimuthal direction, the current filament is still not fully constricted when the maximum current is reached. The filament looks diffuse and wide, which is probably due to the large size of the area in which the initial RF preionization was created.

Figure 4b shows the oscillograms of the voltage U_c at the selected cathode, the currents to the grid I_g and to the anode I_a and the total current $I_\Sigma = I_g + I_a$ recorded in the course of a single plasma filament formation. A high-voltage pulse was applied to the cathode at the moment of maximum preionizing RF voltage equal to about 1.5 kV. Therefore, the voltage on the $U_c(t)$ oscillogram existing prior the breakdown, in fact, is the voltage of the RF generator. Zero time ($t = 0$) on the oscillogram corresponds to the beginning of an increase in voltage at the cathode and correlates with the start of a breakdown.

One can see in Fig. 4b that the filament development is accompanied by an increase in current not only to the anode, but also to the grid. After breakdown, the average currents to the anode and grid are set at approximately 10 and 15 A, respectively, and

their total current remains almost constant over time (see Fig. 5a). The slow decrease in the total current from 25 to 20 A in a time of about 1 ms is due to the discharge of the supply capacitor C. Recording the current waveforms on the anode, I_a, and grid, I_g, with a time resolution of at least 1 μs showed that these currents experience sharp and almost regular antiphase fluctuations, which are especially noticeable at long times after breakdown. These oscillations are characterized by a small amplitude of about $3-5$ A and a quasi-period of about 10 μs (see Fig. 5a). The antiphase of the currents I_a and I_g indicates that the discharge forming the highly conductive plasma filament operates with the pre-set current amplitude determined by the ballast resistance of the external circuit, i.e., the resistance of the plasma filament is low compared to the ballast resistor.

The slow evolution of the plasma filament over long times is shown in Fig. 5b. One can see that after the breakdown is completed, the plasma filament located near the cathode is strongly constricted. This part of the filament has already straightened out compared to its original configuration (see Fig. 4a at $t = 140$ ns) and is oriented exactly along the horizontal cathode–anode line. By the time $t = 5$ μs, diffuse plasma created by preionization still exists around the plasma filament at the cathode and in the rest of the
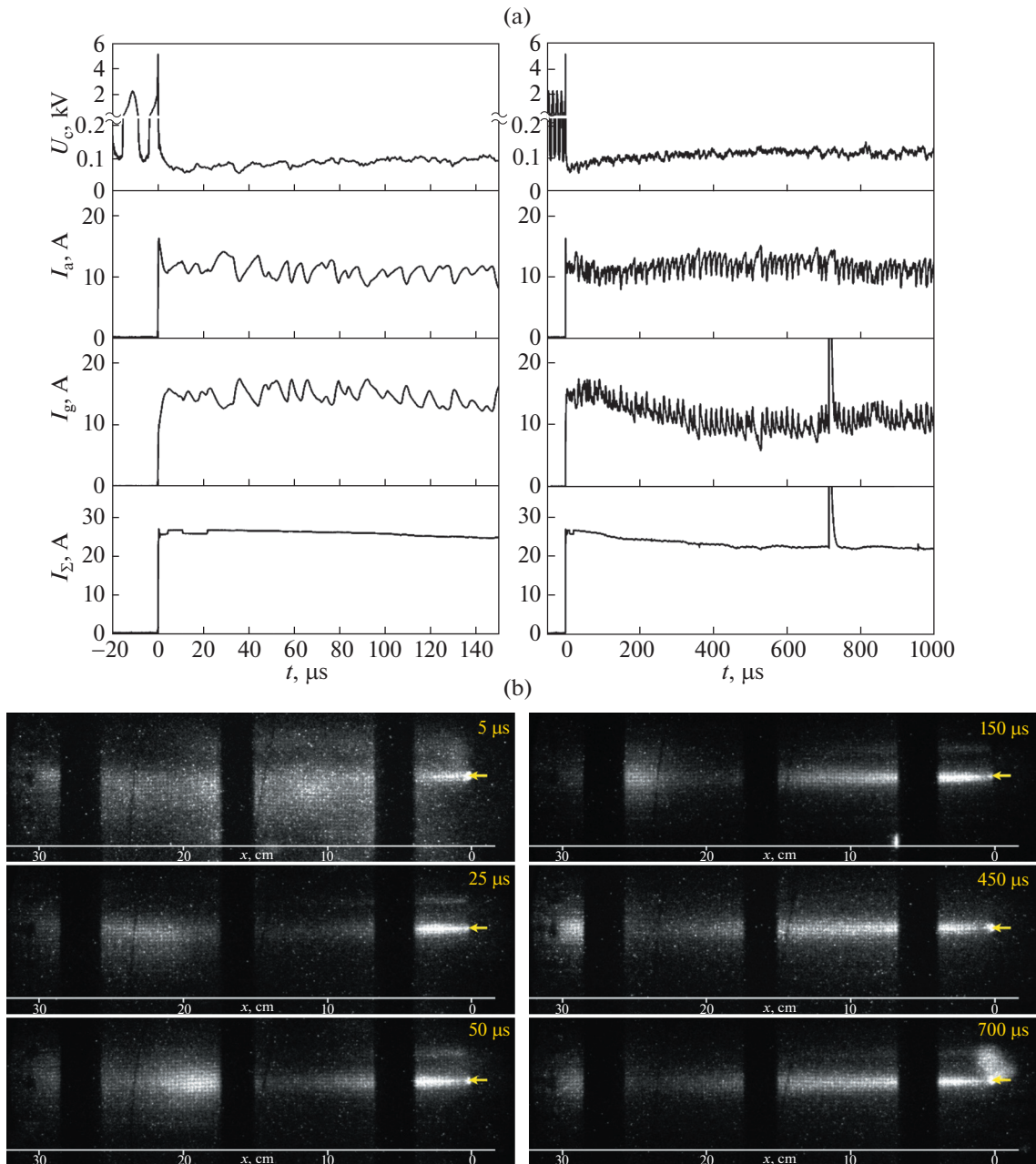
Fig. 5. (a) Oscillograms of the voltage at the cathode U_c and currents I_g and I_a at short and long times during the formation of a single plasma filament; (b) images of the plasma filament at the post-breakdown stage for six time points. The yellow arrow shows the position of the cathode.

gas discharge region. Next, the diffuse plasma disappears, simultaneously accompanied by a rapid elongation of the constricted plasma from the cathode, and a slow oncoming movement of a wider plasma filament from the anode. After the leading edge of the plasma filament from the cathode meets the diffuse plasma from the anode, the cathode filament begins to push it back to the anode. The process is completed in about 600 μs from the beginning of the discharge development. At this moment, the leading edge of the cathode

filament approaches the anode, but a small area near the anode with wide and brightly glowing plasma still remains. After this, the structure and dynamics of the plasma filament practically do not change over time. At the same time, practically along the entire length of the plasma filament, its transverse size turns out to be greater than the distance between neighbor cathodes. This gives confidence that when the entire set of cathode elements is connected, the axial inhomogeneity of the plasma cylinder will be minimal.
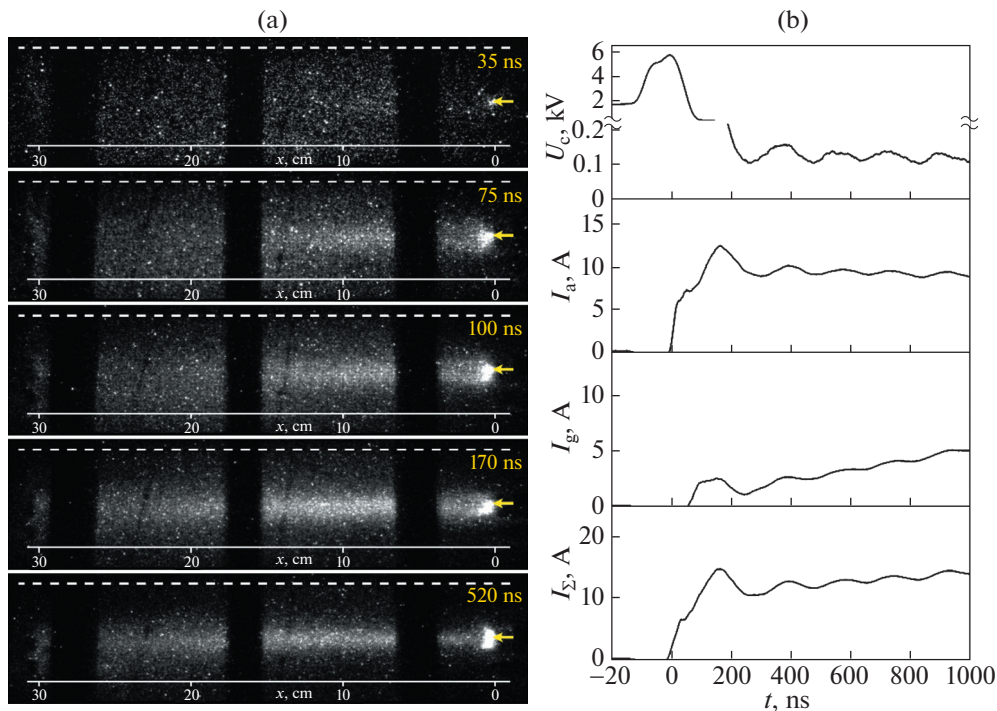
Fig. 6. (a) Five consecutive images of the plasma filament in the process of forming its radial structure. The exposure time of all frames is 60 ns; the yellow arrow shows the position of the cathode; the dotted line is the boundary of the metal grid, (b) oscillograms of voltage at the cathode U_c, currents to the grid I_g, anode I_a, and total current $I_\Sigma = I_g + I_a$. The vertical axis of the voltage on the $U_c(t)$ graph has a gap at a voltage of $U = 0.22$ kV. Argon, $P = 1 \times 10^{-2}$ Torr, $U = -5$ kV, $R = 200$ Ohms.

3.2.2. The dynamics of the radial structure of a single plasma filament. To study this process, the cathode lying in a vertical plane with the axis of the discharge chamber was selected. As can be seen in Fig. 6a, after 100 ns, a clearly defined long plasma filament formed, parallel to the metal grid and located at a distance of only about 3 cm from it. As noted above, the proximity of the plasma filament to the metal grid and the low magnitude of the magnetic induction caused a noticeable current to the grid (Fig. 6b shows this).

3.2.3. Formation of tubular plasma when all cathode elements are connected. An image of the preionizing plasma created by an auxiliary RF discharge inside the GDC when all cathode elements are connected is shown in Fig. 7. Photo-registration was carried out 1 s after switching on the RF discharge. Taking into account the weak glow of the pre-ionizing plasma, the registration was carried out with a frame exposure time of 100 μs and a fully open aperture of the camera lens. This figure shows that, unlike the case with a single connected cathode (see Fig. 4), when all cathodes are connected, the auxiliary RF discharge creates a fairly uniform preionization of the gas both along the whole length of the interelectrode gap and along the azimuth and radius of the discharge chamber almost up to the metal grid. The reason for the latter is that the magnetic field shift of the preionized plasma from any

cathode is compensated by its arrival from a neighboring cathode, etc.

A visual representation of the evolution of the longitudinal and transverse structure of a tubular dis-
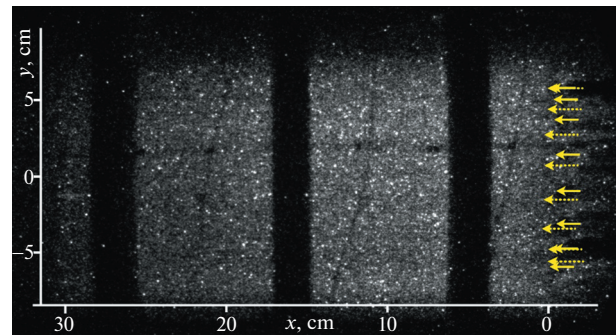
Fig. 7. An image of diffuse plasma of a low-current RF discharge when all the cathodes are switched on. The exposure time of the frame is 100 μs, vertical dark stripes are Helmholtz coils, a spiral dark thin line is a wire on the outer surface of the metal grid, providing mechanical rigidity of the mesh, a thin longitudinal dark line is the place where the grid is soldered. Yellow arrows indicate the position of the cathodes, solid arrows indicate the cathodes closest to the observer; dotted arrows indicate the cathodes farthest from the observer. Argon pressure $P = 1 \times 10^{-2}$ Torr.

charge formed by 16 current filaments is given as a set of photo frames in Tables 1 and 2. The yellow arrows in the photo indicate the positions of the cathodes. The dotted line at the top of each image indicates the border of the grid. The frame shooting time, counted from the moment the high voltage is applied to the cathode, is indicated under each frame. The photographs shown in Table 1 were taken at a voltage pulse amplitude of $U = 5$ kV (left column) and $U = 3$ kV (right column). In this case, the ballast resistors $R = 300$ Ohms for each cathode element were used. Table 2 shows a set of images of a tubular discharge plasma for $U = 5$ kV and for a ballast resistor R of 200 Ohms. The photography conditions (camera lens aperture and exposure time) are indicated on the last frame. We recall that the brighter the light source is, the greater the aperture number is that is selected. This was done to reduce the aperture inlet and limit the luminous flux entering the camera and not blind its receiving matrix.

In the photos shown in Tables 1 and 2 one can see that the evolution of the longitudinal and transverse structure of a tubular discharge consisting of many plasma filaments is generally similar to the evolution of a single filament, as is shown in Fig. 5. The white arrows correspond to the positions of thin dielectric tubes inserted outside the discharge zone in order to give mechanical rigidity to the GDC design. It can only be noted that with lower both the voltage and current, all the processes that determine the dynamics of discharge establishment occur more slowly. The total current is determined by both the applied voltage amplitude U and the magnitude of the ballast resistor R of the individual cathode. As the total current increases, the tubular plasma becomes brighter and more uniform both in length and in azimuthal and radial directions. It has also been recorded that with an increase in the discharge current, local breakdowns occur more often not only from the cathodes to the grid, but also from the lateral surface of the tubular plasma to the grid. This phenomenon is clearly visible in the photographs of Table 2, which correspond to the discharge with the maximum current.

4. DISCUSSION

4.1. The First (Local) Approach to Creating Pre-Ionization

As the experiments have shown, the first (local) method of creating preionization due to auxiliary discharges along the dielectric surface around the cathodes does not provide the necessary reproducibility in time of formation of tubular plasma. One possible reason is related to the influence of the longitudinal magnetic field on the breakdown of the auxiliary discharge, since the current of this discharge is directed perpendicular to the magnetic field. In this case, the trajectories of the electrons are twisted and their

arrival at the auxiliary anode located around the cathode is difficult.

The reduction in the delay time of the breakdown of the auxiliary discharge around one of the cathodes connected simultaneously with the others to the voltage source is explained as follows. The delay time is determined by the probability of seed electrons appearing in the region of a strong field around a separate cathode stressed with high voltage. When a multitude of cathodes are switched on simultaneously, the total size of the region with a strong electric field markedly increases and, thus, the probability of a seed electron appearing in it increases. As a result, the first breakdown occurs quickly in any place in this large area, accompanied by a bright flash of the formed plasma. This breakdown then initiates the breakdown of an auxiliary discharge at neighboring cathodes, presumably due to the photoemission of electrons from the surface of dielectrics around the cathodes. Photoemission occurs owing to the radiation of plasma formed during the breakdown of the first auxiliary discharge and the next ones.
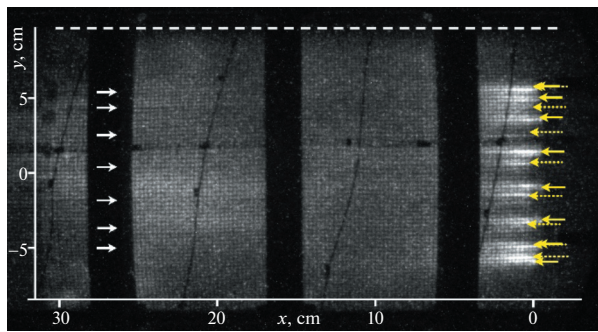
4.2. The Second (Nonlocal or Global) Method to Create Preionization

In the second (nonlocal) method, preionization is created by an RF discharge in the entire volume of the discharge zone up to the surface of the metallic grid. As it turned out, HF preionization provides: (a) a smaller spread in the delay time of the occurrence of the main discharge and (b) its faster development. In the presence of nonlocal preionization, the main discharge occurs almost simultaneously on all cathode elements and develops in about 1 µs after the high-voltage pulse is applied. This time is noticeably less than the time of development of the discharge formed by the first method. Hence, it can be concluded that in the second method of creating tubular plasma, the ionization wave moves faster to the anode. The reason is that the ionization wave moves through a gas well pre-ionized by an RF discharge all the way from the cathode to the anode. The same effect of nonlocal preionization was observed earlier during the propagation of an ionization wave in a capillary tube [8, 9].
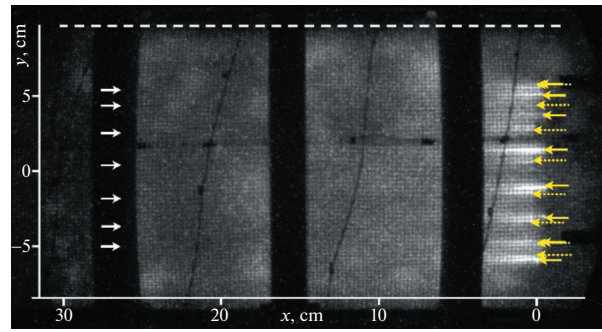
4.3. The Effect of the Radial Electric Field on the Plasma Filament

When studying the dynamics of a single plasma filament in a longitudinal magnetic field, it was found that during its formation, the initially wide filament glow starts to shrink and its light boundary moves slowly away from the grid. Such behavior of the plasma filament formed near the metal grid is not evident because of the existence of the radial electric fields between the filament and the grid, which, it would seem, should have shifted the filament glow to the grid. However, this does not happen, since the longi-
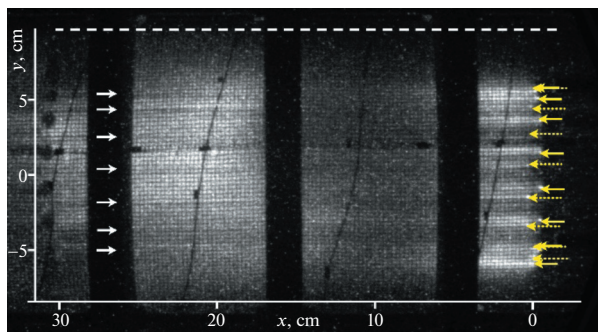
Table 1. Photos of a tubular discharge at different points in time at a pulse voltage of $U = 5$ kV (left column) and $U = 3$ kV (right column). $R = 300$ Ohms
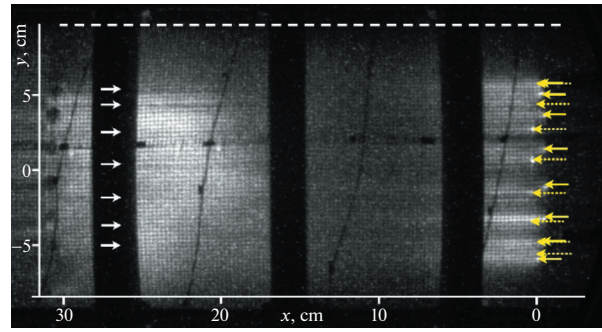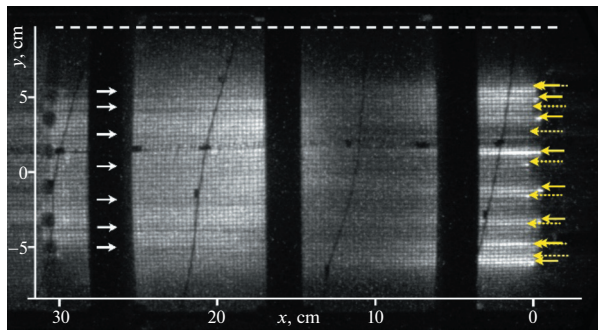

$t = 10$ μs

$t = 10$ μs

$t = 30$ μs

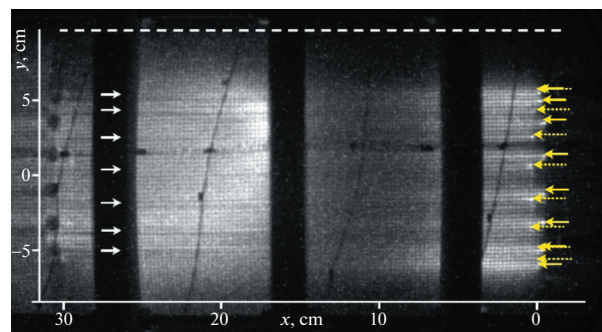$t = 30$ μs

$t = 60$ μs

$t = 60$ μs

$t = 100$ μs
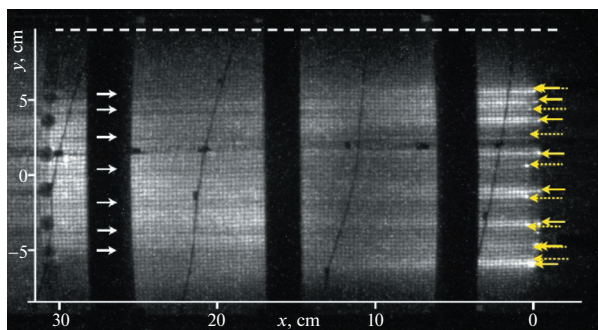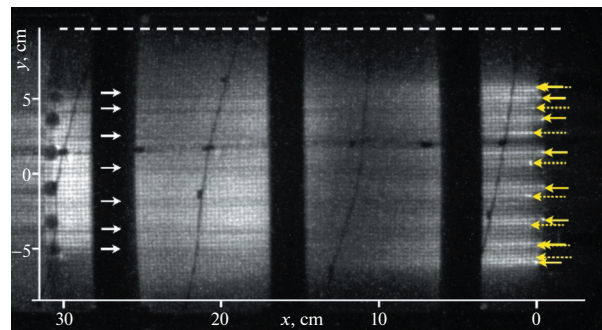
$t = 100$ μs

Table 1. (Contd.)

$t = 200$ μs

$t = 200$ μs

$t = 500$ μs

$t = 500$ μs

$t = 800$ μs

$t = 800$ μs
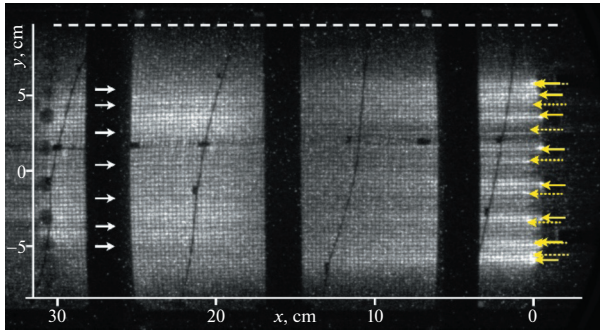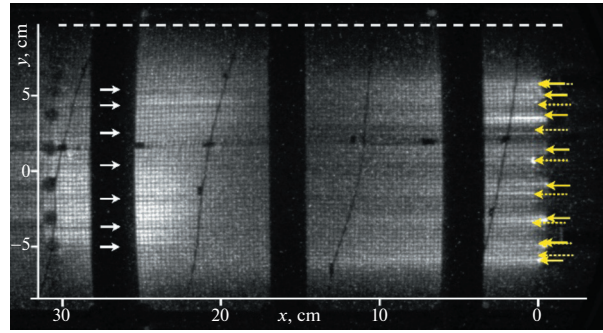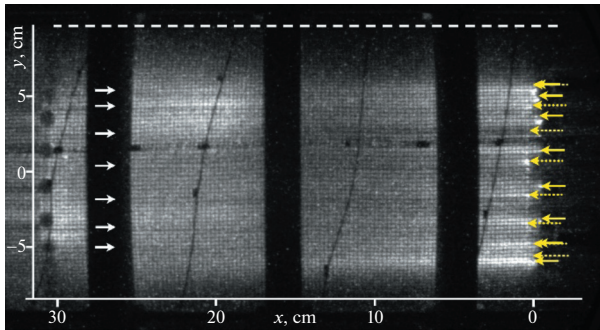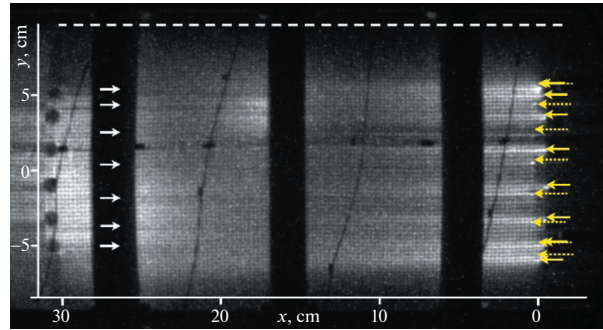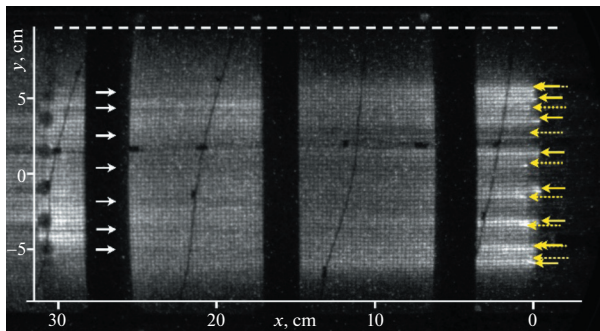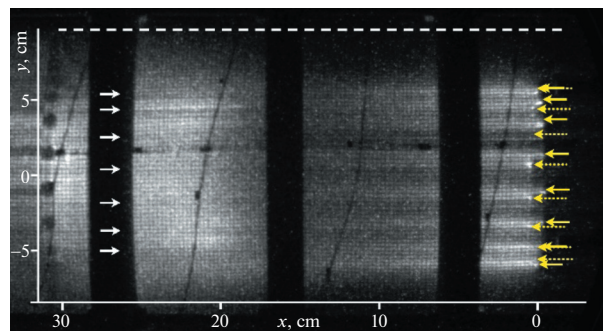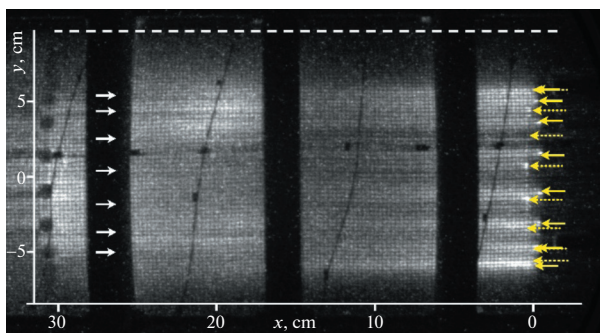
$t = 1100$ μs
aperture 5.6, exposure 1 μs
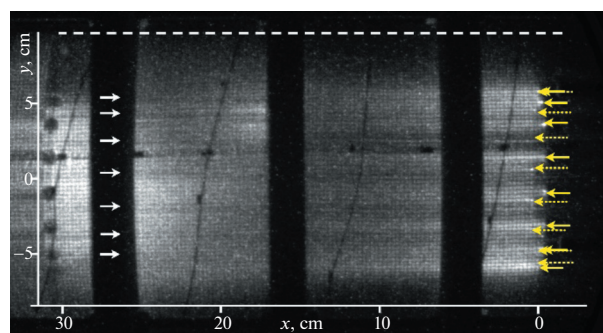
$t = 1100$ μs
aperture 2.8, exposure 1 μs

Table 2. Photographs of tubular plasma at different time points at $U = 5$ kV and $R = 200$ Ohms. The discharge currents correspond to Fig. 6
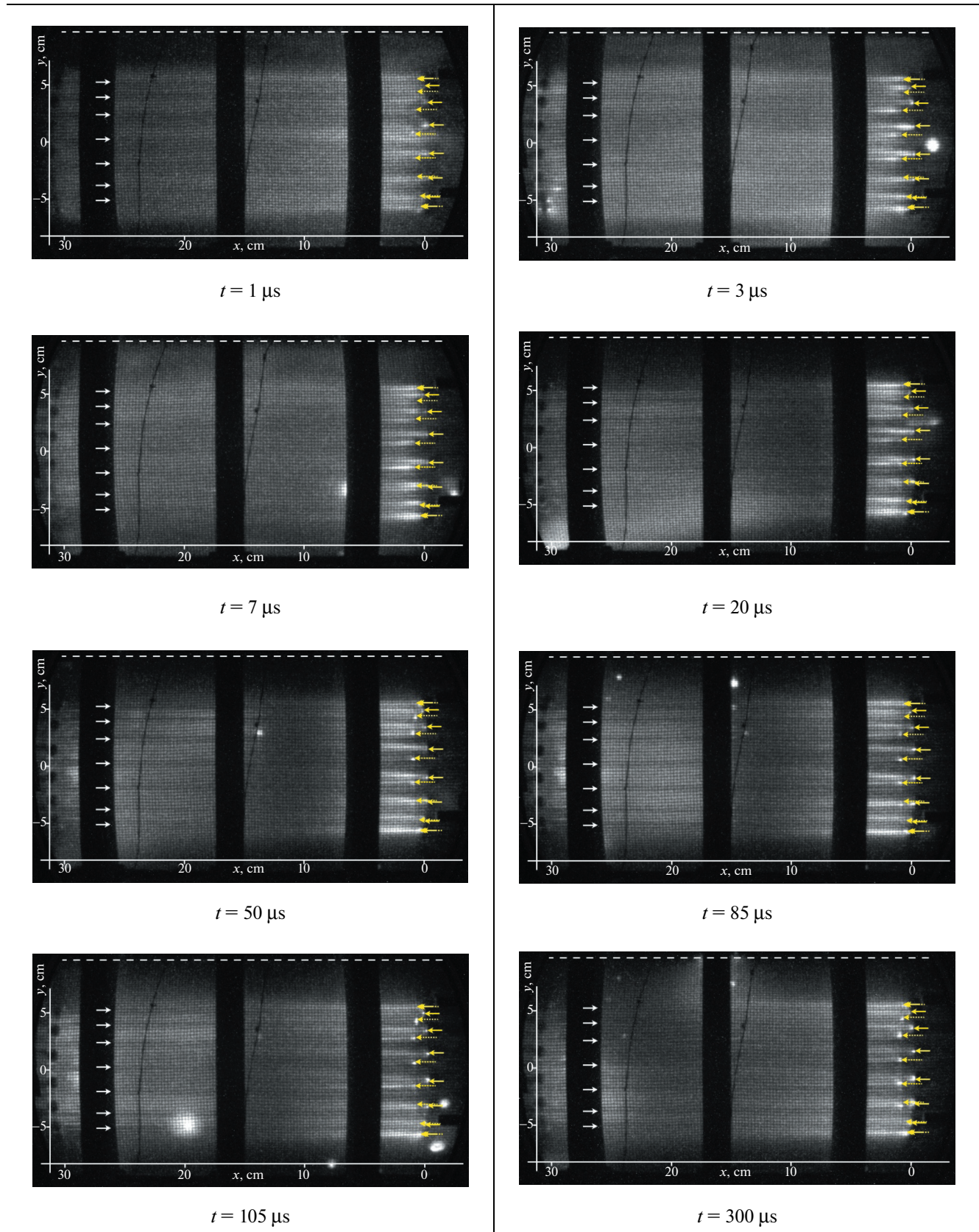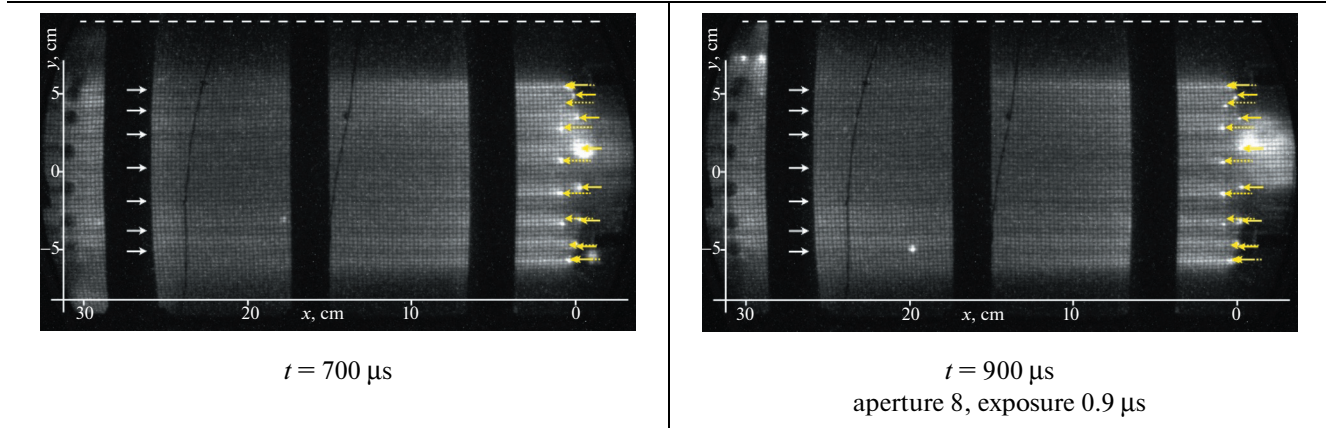

$t = 1$ μs

$t = 3$ μs

$t = 7$ μs

$t = 20$ μs

$t = 50$ μs

$t = 85$ μs

$t = 105$ μs

$t = 300$ μs

Table 2. (Contd.)

$t = 700$ μs

$t = 900$ μs
aperture 8, exposure 0.9 μs

tudinal magnetic field significantly reduces the plasma transfer coefficients in the radial direction, and also "compresses" the electron energy distribution function (EEDF). A reduction of numbers of fast electrons in the EEDF leads to diminishing both the intensity of the electron excitation of atoms and ionization frequency along the radius [10−18]. The latter effect also depends on the strength of the radial electric field, E_r. Therefore, it is of interest to evaluate the structure of the electric field in the discharge zone of the GDC after the formation of a conductive plasma cylinder in it, at least qualitatively.

For this purpose, calculations of the two-dimensional distribution of the electric field were performed under the assumption that the potential on the surface of the plasma cylinder varies linearly along its length, while the inner surface of the GDC metal housing is equipotential and grounded. The results of 2D calculations are shown in Fig. 8. As can be seen in this figure, there is a sufficiently strong radial field strength E_r around the plasma cylinder, which decreases as it moves away from the cathode. However, even at three-quarters of the length of the tubular plasma measured from the cathode, E_r is still not zero. The radial field transfers part of the current from the tubular plasma to the grid, i.e., to the housing of the GDC, and the closer to the cathode, the greater the magnitude of this current.

The presence of a radial current and a longitudinal magnetic field can also lead to rotation of the plasma cylinder. In this case, the angular velocity of rotation proportional to E_r may not be the same along the plasma cylinder. In this regard, it is appropriate to recall the quasi-periodicity of low-current local breakdowns from the cathode to the grid that were observed in the experiment. They may be associated with the removal of the formed highly conductive plasma from the breakdown zone by an Ampere force F, which is proportional to the current $\vec{j_\perp}$ and magnetic induc-

tion $\vec{B}$: $F \sim [\vec{j_\perp} \times \vec{B}]$. In this case, the removal of this plasma creates conditions for a new local breakdown.

It is important to note that the two-dimensional structure of the electric field in the presence of tubular plasma always forms while not depending on the method of plasma creation. In this case, it is very likely that the above effects due to the 2D structure of the electric field (i.e., the current on the metal wall of the GDC and rotation of the tubular plasma) can lead to a change in the parameters of the tubular plasma in the longitudinal direction. This should be taken into account when using the plasma source in question in practice.

The measured values of the anode current and voltage drop along the plasma cylinder allow us to estimate the amount of Joule energy released by the discharge. It is estimated that, on average, on each gaseous particle at the time $t = 1$ ms there is an energy of about 1 eV or more. This is a high value, which indicates that the tubular plasma can be completely ionized and be in local thermodynamic equilibrium.

5. CONCLUSIONS

Summarizing the results presented on the creation of extended ($l = 30$ cm) tubular plasma in argon at pressures of $10^{-2}-10^{-3}$ Torr and in a weak longitudinal magnetic field, we can say the following. The experiment showed that both methods are capable to form sufficiently uniform tubular plasma in length and azimuth, consisting of separate and overlapping diffusive plasma filaments. Moreover, this plasma is well isolated by a weak magnetic field from the metal wall and is kept from it at a distance of about 35 mm.

The first method using local preionization ensured the formation of the required plasma at amplitudes of applied voltage ranging from 3 to 5 kV. Its disadvantage is that the plasma was formed with an uncontrolled and unacceptable delay ranging from 90 to 20 μs. In addition, this method is quite complicated from the point of view of its technical implementation, requir-
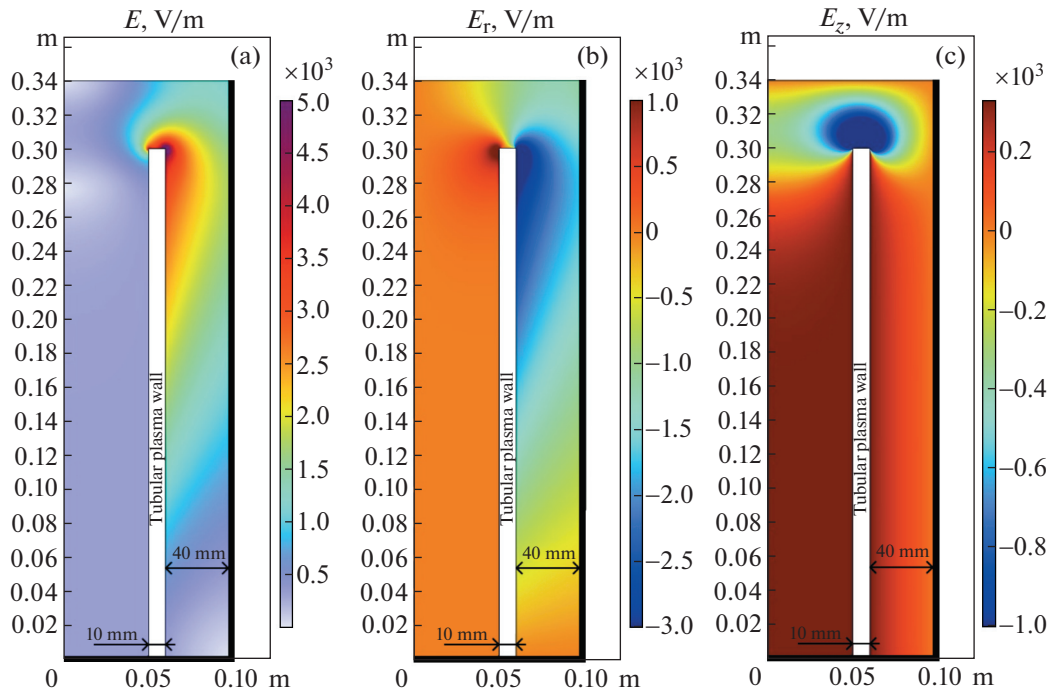
Fig. 8. The two-dimensional structure of the axially symmetric electric field between the tubular plasma and the metal wall of the GDC (longitudinal section). The voltage drop along the plasma is 100 V. The cathode is at the top, the anode is at the bottom. (a) The modulus of the electric field strength; (b) the radial component of the electric field; (c) the longitudinal (along the magnetic field) component of the electric field. The black line shows a grounded boundary at which the potential is zero.

ing the use of a large number of high-voltage and high-current pulse circuits, which are individual for each element of the sectioned cathode.

The second method of creating a tubular plasma using an auxiliary RF discharge turned out to be simpler in execution and more stable and robust in terms of repeatability of the results. An acceptable plasma is obtained at a pulse voltage amplitude of $U = 5$ kV and a ballast resistor at each cathode of $R = 200$ Ohms. In this mode, the voltage drop along the tubular plasma is about 110 V with average electric field strength in the plasma of about 4 V/cm. Voltage drops on the cathode and anode layers were not taken into account when estimating the average field strength.

The total discharge current passing through the tubular plasma to the anode and partially collected by the metallic wall is about 260 A. With the above parameters, the discharge is sufficiently stable with respect to low-current breakdowns on a closely located metal wall of the GDC. At the same time, longitudinal and azimuthal uniformity is maintained in the tubular plasma at least for 1 ms. It is estimated that the average current density in a tubular plasma is about 2 A/cm^2 at an electron density of 10^{13} cm^{-3} and their temperature is about 1 eV. To clarify these values, direct measurements are needed, which are planned to be carried out in the future.

CONFLICT OF INTEREST

The authors of this work declare that they have no conflicts of interest.

OPEN ACCESS

REFERENCES

1. L. S. Bogdankevich, M. V. Kuzelev, and A. A. Rukhadze, Sov. Phys.—Usp. **24**, 1 (1981).
https://doi.org/10.3367/10.1070/PU1981v024n01ABEH004606

2. P. S. Strelkov, Phys.—Usp. **62**, 465 (2019).
https://doi.org/10.3367/UFNe.2018.09.038443

3. A. B. Buleyko, A. V. Ponomarev, O. T. Loza, D. K. Ulyanov, and S. E. Andreev, Phys. Plasmas **28**, 023303 (2021).
https://doi.org/10.1063/5.0031432

4. A. B. Buleyko, A. V. Ponomarev, O. T. Loza, D. K. Ulyanov, K. A. Sharypov, S. A. Shunailov, and M. I. Yalandin, Phys. Plasmas **28**, 023304 (2021).
https://doi.org/10.1063/5.0031432

5. I. N. Kartashov and M. V. Kuzelev, Plasma Phys. Rep. **47**, 548 (2021).
https://doi.org/10.1134/S1063780X2106009X

6. Yu. Akishev, V. Karalnik, I. Kochetov, A. Napartovich, and N. Trushkin, Plasma Sources Sci. Technol. **23**, 054013 (2014).
https://doi.org/10.1088/0963-0252/23/5/054013

7. G. A. Mesyats and Y. D. Korolev, Sov. Phys. Usp. **29**, 57 (1986).
https://doi.org/10.3367/UFNr.0148.198601e.0101

8. Yu. Akishev, T. Alekseeva, V. Karalnik, and A. Petryakov, J. Phys. D: Appl. Phys. **55**, 145202 (2022).
https://doi.org/10.1088/1361-6463/ac45af

9. Yu. S. Akishev, V. B. Karal'nik, A. V. Petryakov, and Yu. Z. Ionikn, Plasma Phys. Rep. **47**, 60 (2021).
https://doi.org/10.1134/S1063780X21010013

10. G. J. M. Hagelaar and L. C. Pitchford, Plasma Sources Sci. Technol. **14**, 722 (2005**).**
https://doi.org/10.1088/0963-0252/14/4/011

11. N. L. Starikovskiy, M. N. Aleksandrov, and M. N. Shneider, Plasma Sources Sci. Technol. **32**, 035005 (2023).
https://doi.org/10.1088/1361-6595/acc053

12. S. T. Surzhikov and J. S. Shang, Plasma Sources Sci. Technol. **23**, 054017 (2014).
https://doi.org/10.1088/0963-0252/23/5/054017

13. S. T. Surzhikov and J. S. Shang, in *Proceedings of the 45th AIAA Plasmadynamics and Lasers Conference, Atlanta, GA, 2014,* Paper AIAA 2014-2236.

14. S. T. Surzhikov, Plasma Phys. Rep. **43**, 363 (2017).
https://doi.org/10.1134/S1063780X17030138

15. S. Gao, S. Chen, Z. Ji, W. Tian, and J. Chen, Adv. Math. Phys. **2017**, 9193149 (2017).
https://doi.org/10.1155/2017/9193149

16. A. I. Ryakhovskiy, A. A. Schmidt, and V. I. Antonov, Tr. Inst. Sist. Program. Ross. Akad. Nauk **29** (6), 299 (2017).
https://doi.org/10.15514/ISPRAS-2017-29(6)-19

17. I. M. Ulanov and V. A. Pinaev, High Temp. **52**, 26 (2014).
https://doi.org/10.1134/S0018151X14010209

18. S. Gao, J. Feng, W. Li, and J. Cai, Eur. Phys. J. Appl. Phys. **88**, 30801 (2019).
https://doi.org/10.1051/epjap/2019190224